Available online at www.sciencedirect.com
ScienceDirect
Proceedings of the Combustion Institute xxx (2010) xxx–xxx
Proceedings of the Combustion Institute
www.elsevier.com/locate/proci

LES study of cycle-to-cycle variations in a spark ignition engine

B. Enaux [a,b], V. Granet [a,c], O. Vermorel [a,*], C. Lacour [d], C. Pera [d], C. Angelberger [d], T. Poinsot [e]

[a] CERFACS, CFD Team, 42 Avenue G. Coriolis, 31057 Toulouse Cedex 01, France
[b] PSA Peugeot Citroën – DRIA, 2 Route de Gisy, 78943 Velizy-Villacoublay Cedex, France
[c] Renault SAS, 1 Avenue du Golf, 78288 Guyancourt Cedex, France
[d] IFP, 1& 4 Avenue de Bois-Préau, 92852 Rueil-Malmaison Cedex, France
[e] Institut de Mécanique des Fluides de Toulouse, CNRS, Avenue C. Soula, 31400 Toulouse, France

Abstract

Multi-cycle Large Eddy Simulation (LES) of flow and combustion in a single cylinder engine set-up are presented in order to validate the ability of this technique to reproduce cyclic combustion variability in a spark ignition engine. The simulated engine operating point is part of a larger experimental database acquired at IFP and specifically designed to validate LES techniques in terms of cycle-to-cycle prediction. To characterize individual cycles, the database combines acquisitions of pressure and temperature in different locations of the engine set-up with optical diagnostics in the intake pipe and the cylinder. This new experimental database combined with LES is a powerful tool to study cycle-to-cycle variations (CCV). The operating points include points with low and high CCV levels. The LES includes the whole engine set-up, and covers 25 consecutive four-stroke engine cycles for a reference operating point with low CCV. The results show that LES is able to reproduce the experimental findings, and illustrate how LES can help explain the sources of CCV. In the present case it is shown that CCV are essentially due to velocity fluctuations at the spark plug, which induce variations of the early flame kernel growth and of the overall combustion duration.

Keywords: Large Eddy Simulation; Cyclic combustion variations; Spark ignition; Multi-cycle engine simulation; Premixed combustion

1. Introduction

Instabilities are the heart of many present research efforts in gas turbines [1–4] or piston engines [5,6]. Cycle-to-cycle variations (CCV) in piston engines are detrimental in terms of combustion efficiency. Understanding and controlling CCV is thus an essential step to further optimize overall engine efficiency. The difficulty is that many different mechanisms can lead to CCV, and that their importance and interactions can hardly be studied using only standard engine experiments based on cylinder pressure analysis.

The recent development of Large Eddy Simulation (LES) tools has opened new perspectives in this field: computations of multiple cycles in piston engines [5–8] have demonstrated the potential of LES in terms of studying CCV. A major

* Corresponding author. Fax: +33 (0) 5 61 19 30 00.
E-mail address: vermorel@cerfacs.fr (O. Vermorel).

1540-7489/$ - see front matter © 2010 The Combustion Institute. Published by Elsevier Inc. All rights reserved.
doi:10.1016/j.proci.2010.07.038

shortcoming of these studies was the lack of dedicated experimental data for validating the performed LES studies in terms of their ability to accurately describe the physical phenomena participating to CCV. Another difficulty was the simulation of a sufficiently high number of engine cycles to be able to access statistical information that could be compared with experiments.

In the present work, parallel LES was used to simulate 25 consecutive cycles of the reacting flow in a single cylinder engine set-up for which dedicated experimental data were acquired. In order to limit the uncertainties resulting from boundary conditions, the LES spans the whole engine set-up: intake plenum and pipes, cylinder, exhaust pipes and plenum. In the experiments, the engine was fuelled with a controlled mixture of gaseous propane and air, mass flow rates being controlled using sonic nozzles. This set-up provides simple and accurate boundary conditions for the simulation: the mean flow rates are carefully monitored by the sonic nozzles while the plenums impose almost constant pressure conditions for the LES boundary conditions. The engine was instrumented with multiple pressure and temperature transducers to monitor in a cycle-resolved manner the flow all along the engine set-up. Optical diagnostics in the intake duct and the cylinder allowed to characterize the flow and combustion in the cylinder. Acquired engine operating points include both stable points (i.e., with low levels of CCV) and unstable points (i.e., with high levels of CCV). The objective of the experiment is to build a database to validate LES and its ability to accurately reproduce CCV. The presented work is a first contribution in this direction, aiming at validating the predictive capability of LES on a reference stable operating point.

Section 2 presents the configuration while Section 3 describes the LES solver and models. Results (acoustic wave identification, pressure variability, cyclic variation mechanisms) are presented in Section 4.

2. Configuration

The engine set-up is shown in Fig. 1. The single cylinder spark ignition engine has a four-valve, pent-roof combustion chamber with a flat piston. Various operating points have been acquired, comprising motored and fired operation with low CCV (stable) and high CCV (unstable) levels [9]. The operating point simulated in the present work is a stable fired case fuelled with a gaseous propane/air mixture (Table 1). Air is introduced in a first plenum (not represented in Fig. 1), and mixed with gaseous propane in a second plenum sufficiently large to obtain an homogeneous mixture. Both air and propane flow rates are controlled by sonic nozzles. At the engine exhaust, gases are tranquilized in the exhaust plenum. Close to the mixing and exhaust plenums, a flame-arrestor is added for safety reasons.

One hundred experimental consecutive cycles have been acquired for this operating point. Several diagnostics (particle image velocimetry (PIV), OH laser induced fluorescence (LIF), chemiluminescence) were used to characterize flow and combustion in the cylinder. Instantaneous pressure and temperature signals were recorded in a cycle-resolved way along the intake (probes 1, 2 and 3) and exhaust ducts (probe 4).

3. Numerical approach and methodology

3.1. LES solver and grids

Computations are performed with the AVBP code [10]. AVBP is a fully compressible and explicit

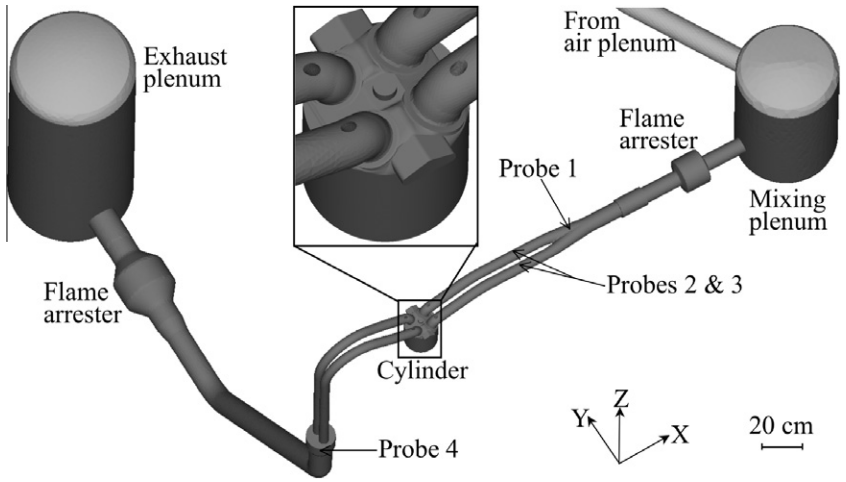

Fig. 1. Experimental set-up and computational domain. Pressure transducer locations are shown by the arrows.

Please cite this article in press as: B. Enaux et al., *Proc. Combust. Inst.* (2010), doi:10.1016/j.proci.2010.07.038

Table 1
Characteristics of the engine. Crank Angle Degrees (CAD) are relative to combustion Top-Dead-Center (TDC).

	Unit	Value
Compression ratio	[-]	9.9
Rotational speed	[rpm]	1200
Bore	[mm]	82
Stroke	[mm]	83.5
Connecting rod length	[mm]	144
Intake Valve Opening (IVO)	[CAD]	350
Intake Valve Closure (IVC)	[CAD]	−120
Exhaust Valve Opening (EVO)	[CAD]	120
Exhaust Valve Closure (EVC)	[CAD]	−350
Spark timing	[CAD]	−20

code that solves the multi-species Navier–Stokes equations with realistic thermochemistry on unstructured grids. Convection terms are discretized using a finite volume Lax-Wendroff scheme [11]. Sub-grid stresses are modeled by a classical Smagorinsky model [12]. The moving grid management is handled by an Arbitrary Lagrangian Eulerian method combined with a Conditioned Temporal Interpolation technique [13].

The present computation covers 18 720 Crank Angle Degrees (CAD) i.e. 26 consecutive cycles including intake, compression, expansion and exhaust strokes. For each cycle, 41 grids are used to handle moving boundaries. A second-order scheme [13] is used to interpolate the solution for each grid topology change. The smallest grids (~2.2 million tetrahedral cells) are found around TDC, the largest (up to 9.6 million cells) are used to describe the intake and exhaust valve closures. This method allows to limit the grid deformation while maintaining a spatial resolution Δx close to 0.8 mm in the cylinder during the whole cycle. Numerical and precision issues are discussed in [5] and [14].

The computational domain extends from the mixing plenum, where a perfect propane/air mixture is assumed, to the exhaust plenum where burnt gases are ejected. Pressure is imposed [10,15] at the top of the mixing and exhaust plenums (Fig. 1). The target pressures are time-varying signals extracted from experimental data. They typically stay very close to the mean of 0.4 bar at the mixing plenum and 1 bar at the exhaust plenum. Compared to previous simulations, where the domain only covered a part of the intake/exhaust ducts [5,6,8], this computational domain greatly simplifies the definition of the boundary conditions. Back-flow phenomena occurring in the intake and exhaust lines are naturally damped within the plenums and do not have to be accounted for at the boundaries of the present domain. Walls are handled using a logarithmic law-of-the-wall formulation for velocity and temperature [3]. Note that this methodology has already been applied and validated on a motored engine operating point [16].

The CPU time is approximately 1.4 day per cycle on 400 processors of a SGI Altix ICE 8200 cluster.

3.2. Flame-arrestor

Accounting in the LES for the flame-arrestors installed in the experiment was found to be mandatory, as they strongly affect the acoustic behavior of the whole system. These devices contain several hundreds of small channels of 0.5 mm diameter (porosity $\sigma = 0.68$), which are too small for LES. Their effect was thus modeled using the approach of Mendez and Eldredge [17], which prescribes a discharge law to evaluate the pressure drop and the acoustic transfer matrix through a porous device as a function of the bulk velocity and a discharge coefficient C_D. Preliminary tests have shown that the model allows to recover the correct impedance of the flame-arrestors as well as the pressure losses over a wide range of velocity.

3.3. Combustion modeling

Combustion is modeled using Arrhenius type reaction rates. A reduced two-step chemical scheme (called C3H8-BE2 in the rest of the manuscript) accounting for five species is used to describe propane/air chemistry:

$$C_3H_8 + 3.5O_2 \rightarrow 3CO + 4H_2O \quad (1)$$

$$CO + 0.5O_2 \rightleftharpoons CO_2 \quad (2)$$

Reaction (1) controls the flame speed while the CO—CO_2 equilibrium allows to accurately reproduce the flame temperature. The forward reaction rates for these two reactions read:

$$k_{f,1} = A_1 e^{\left(\frac{-E_{a,1}}{RT}\right)} [C_3H_8]^{n_{C_3H_8}} [O_2]^{n_{O_2,1}} \quad (3)$$

$$k_{f,2} = A_2 e^{\left(\frac{-E_{a,2}}{RT}\right)} [CO]^{n_{CO}} [O_2]^{n_{O_2,2}} \quad (4)$$

A_j and $E_{a,j}$ are the pre-exponential factor and the activation energy of reaction j ($j = 1, 2$) and n_k is the reaction exponent for species k (Table 2).

Table 2
Arrhenius parameters for the C3H8-BE2 scheme.

	C_3H_8 oxidation		CO—CO_2 equ.	
E_a [cal/mol]	3.4×10^4		1.2×10^4	
A [cm^3/mol s]	5.8232×10^{12}		2.0×10^9	
Reaction exponents [–]	$n_{C_3H_8}$	0.8	n_{CO}	1.00
	$n_{O_2,1}$	0.86	$n_{O_2,2}$	0.50

Please cite this article in press as: B. Enaux et al., *Proc. Combust. Inst.* (2010), doi:10.1016/j.proci.2010.07.038

This reduced scheme is built to recover the laminar flame speed and the adiabatic temperature at stoichiometry and for pressure and temperature ranges representative of the operating point. Figure 2 compares the laminar flame speed S_L^0 and the adiabatic temperature T_{adia} predicted by the C3H8-BE2 scheme with the power law of Metghalchi and Keck [18], the detailed mechanisms of Jerzembeck et al. [19] and the Gri-Mech 3.0 [20]. The ranges of pressure and temperature used in abscissa mimic an isentropic evolution of fresh gases from a reference state representative of ignition conditions $P_{ign} = 5.44$ bar, $T_{ign} = 723$ K. It is worth mentioning that neither [18] nor [19] show results for such high pressures and temperatures. In [18], the maximum fresh gases temperature is 750 K. S_L^0 values presented in Fig. 2 are therefore extrapolated values from a simple power law and coefficients given in this paper (see Eq. (14) and Table 2 in [18]). In [19], results are given for a pressure up to 5 atm. Therefore, values shown in Fig. 2 are the results of new CANTERA [21] calculations using the full chemical kinetic mechanism validated in [19]. Figure 2 shows that C3H8-BE2 correctly reproduces the pressure and temperature dependence of the laminar flame speed and the adiabatic temperature from 5 to 20 bars.

Flame/turbulence interactions are taken into account by the dynamically thickened flame model [22]. Ignition is described via the energy deposition model [23,24]. During the ignition phase, thickening is not activated and begins only when the flame starts propagating. The spark is replaced by a volumetric source term added to the energy equation. The source term distribution is Gaussian in time and space. The deposit lasts about 100 μs and the deposit diameter is 2.5 mm long. The total energy transmitted to the gas is 20 mJ, which corresponds to 10% of the overall energy provided by the electrical spark. This percentage is a classical estimate considering losses due to thermal conduction to the electrodes, radiation and shock wave expansion [25,26]. In order to solve the early kernel propagation, the mesh is specifically refined around the deposition spot ($\Delta x = 0.2$ mm).

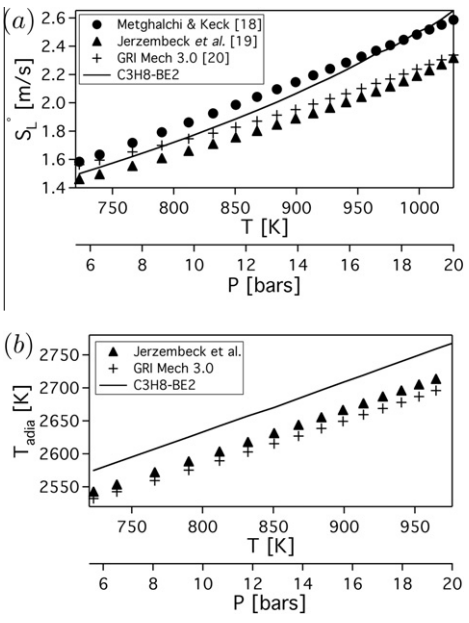

Fig. 2. Laminar flame speed (a) and adiabatic temperature (b) obtained with C3H8-BE2 for an isentropic compression.

4. Results and discussion

Starting from a preliminary motored engine computation, the computation covers 26 consecutive cycles. The criteria used to assess the convergence of the simulation are both the trapped mass in the cylinder and the internal burnt gases recirculation rate. Figure 3 shows the total trapped mass in the cylinder and the internal gas residuals (IGR) for the 26 cycles. The total mass stabilizes from cycle 2 very close to the experimental value of 181 mg estimated with a system simulation approach [9]. The IGR are shown to account for about 12.5% of the total mass, close to the experimental value of 9.6%. Note that the variations in IGR are much higher ($\sim 10\,\%$) than the variations in trapped mass ($< 1\%$). The first cycle mass is obviously much larger than the other cycles because it is not initialized correctly (unlike the 25 others). Therefore, only the last 25 cycles are considered hereafter and cycle 1 will actually refer to the second simulated cycle.

4.1. Acoustic behavior

One of the main advantages of this configuration is to completely account for acoustics. The phase-averaged pressure signals at probes 1, 2 and 3 show that the LES correctly reproduces the experimental acoustic behavior in the intake ducts during the whole cycle. Figure 4a shows

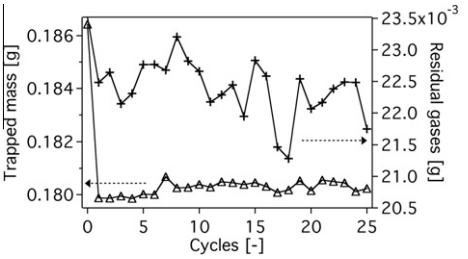

Fig. 3. Total trapped mass (△) and residual gases mass (+) in the cylinder for the 26 LES cycles.

Please cite this article in press as: B. Enaux et al., *Proc. Combust. Inst.* (2010), doi:10.1016/j.proci.2010.07.038

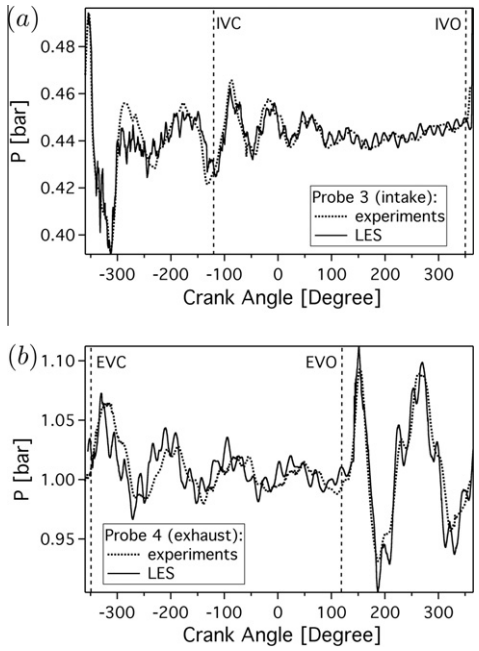

Fig. 4. Phase-averaged crank-resolved pressure at probes 3 (a) and 4 (b) (see Fig. 1 for probe positions).

the pressure evolution at probe 3 and confirms that the acoustics in the intake pipes are correctly captured by the LES (probes 1 and 2 show very similar results but are not shown for the sake of concision). The damping of the signal from IVC to IVO, i.e. when the intake valves are closed, is well reproduced by the computation.

However, LES also exhibits a high frequency component at 420 *Hz* not present in the experiments. Additional computations using the Helmholtz solver AVSP [27] revealed that this frequency is neither a hydrodynamic mode nor a numerical artifact, but a real acoustic mode, the five-quarter wave mode of the complete intake line. At this point, no information allows to assert with certainty why this acoustic mode is damped in the experiments and not in the LES. It is however expected that these differences will not affect the conclusions. Comparisons at probe 4 located in the exhaust duct (Fig. 4b) allow to draw the same conclusions. Note that the modeling of the flame-arrestors is of primary importance to correctly predict the pressure evolution both in the intake and exhaust lines [16]. Preliminary computations without flame-arrestors showed a noticeable shift in phase and insufficient damping.

4.2. Indicators of in-cylinder variability: pressure and burnt mass fraction (BMF)

Figure 5 displays the temporal evolution of the in-cylinder pressure, in terms of phase-averaged

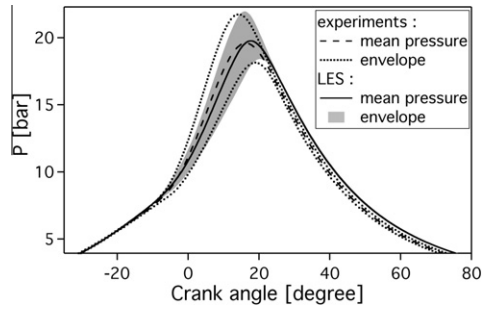

Fig. 5. Comparison of experimental and LES cylinder pressure.

value P_{mean} and envelope. The pressure envelope delineates the zone where 95% of the cycles are included and is defined as $P_{\text{mean}}(t) \pm 2\sigma_P$ with σ_P the pressure standard deviation. The agreement between LES and experiments is satisfactory. Although the number of simulated cycles is too small to be fully representative, the amplitude of the statistical envelopes is quite similar, indicating that the cyclic variability of the experiment is captured by the LES. However, a slight temporal shift is visible during the expansion stroke, both for the envelope and the mean value. This shift is also noticeable in Fig. 6 which shows the temporal evolution of the BMF, in terms of phase-average value and envelope. Both experimental and LES curves are here extracted from a classical 0D combustion analysis tool. The amplitude of the statistical envelopes is once again comparable. The consumption rates are very similar in the experiment and in the LES during the first 15 CAD and slightly drift apart afterwards. This shift in the combustion process partly explains the delay observed on the pressure curves. Another reason could come from an erroneous estimation of the wall temperatures, which are difficult to characterize accurately in the experiments.

Another way to highlight CCV is to plot the maximum pressure of cycle $n+1$ versus the maximum pressure of cycle n. Indeed, in-cylinder peak pressure is a classical indicator of cycle-to-cycle variations [28]. Figure 7 confirms that the range

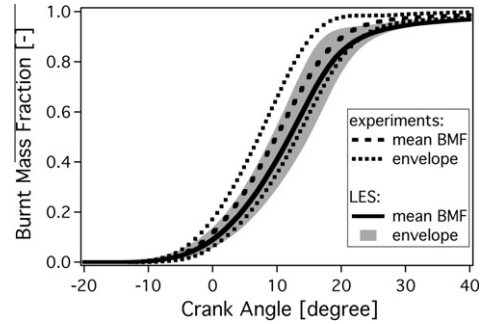

Fig. 6. Comparison of experimental and LES BMF.

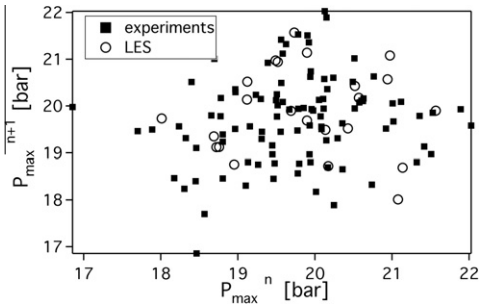

Fig. 7. Maximum cylinder pressure of cycle $n+1$ versus maximum cylinder pressure of cycle n.

of combustion variation is similar in the experiments and in the LES. The mean pressure peak and its standard deviation are in close agreement: 19.87 bar and 0.91 bar for the LES versus 19.73 bar and 0.93 bar for the experiments. The relative variation in peak pressure is small in both cases (4.6% and 4.7%, respectively) confirming that this operating point may be considered as stable. No apparent correlation exists between a cycle and the following one. The sequence of cycles seems completely random, without convergence towards a single cycle.

4.3. Analysis of cycle-to-cycle combustion variations

The observed pressure variability is a direct consequence of variations in the flame development. The evolution of the resolved LES flame surface (measured by the area of the progress variable $c = 0.5$ iso-surface) shown in Fig. 8 confirms the cyclic variability of the combustion process. The grey area represents the statistic envelope of the 25 individual cycles. For the sake of clarity, only three typical individual cycles are explicitly shown (cycles 14, 15 and 16). Although these three cycles are consecutive, they exhibit noticeably different behaviors in terms of peak pressures, reaching, respectively, 20.98 bar, 21.08 bar and 18.01 bar. The combustion process shows different stages which can be highlighted using the classical indicators CA2, CA10, CA50 and CA90, where CAX is the period during which the burnt mass fraction reaches X%. The first phase delineated by the CA2 is the initial flame development stage. The second phase may be considered as a phase of free turbulent propagation: the flame front is located under the cylinder head, mainly on the exhaust side, and the interactions with the walls are limited. On the contrary, the third and fourth phases are characterized by strong interactions with walls, first the piston (phase 3) and then the cylinder liner (phase 4).

The first phase is known to be the most crucial stage with respect to cycle-to-cycle variations [28,29]. This assertion is partly confirmed by the coefficient of variation of the CA2,COV_{CA2}, which is rather high at 5.14%. Moreover, Fig. 9 shows a good correlation between CA2 and CA90 (Pearson correlation coefficient $R_{CA2-CA90} = 0.75$ assuming a linear dependance): a fast (respectively slow) initial flame growth leads most often to a globally fast (respectively slow) combustion cycle. Figure 8 suggests that phase 2 is similar from cycle to cycle, which is confirmed by the high correlation coefficient between CA2 and CA10 $R_{CA2-CA10} = 0.92$. Singular events occur during phase 3 which can largely change the initial trend. This is the case for cycle 14 compared to cycle 15 for example. This variability is clearly underlined by the drop in the correlation coefficient $R_{CA10-CA50} = 0.76$. Finally, phase 4 seems to follow on naturally the third phase and does not introduce additional variability in the combustion process ($R_{CA50-CA90} = 0.94$).

4.4. Factors of cyclic combustion variations

In order to determine the origins of the combustion variations, the emphasis is put on the first phase which was shown to be a key stage. During this phase, the initially laminar spherical flame kernel becomes progressively wrinkled and turbulent. Many factors influence the duration of this phase:

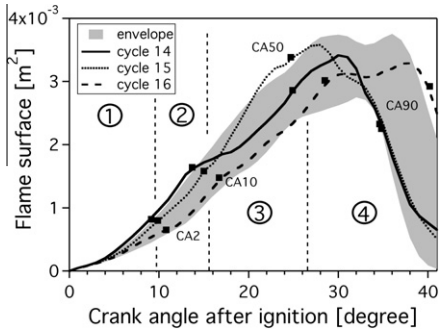

Fig. 8. Evolution of resolved flame surface.

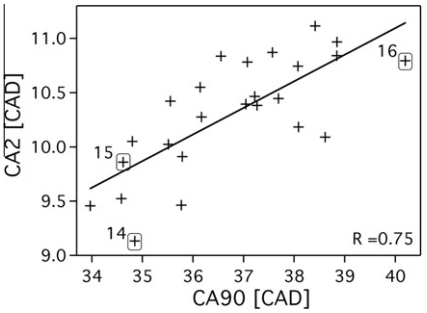

Fig. 9. Correlation between CA2 and CA90.

Please cite this article in press as: B. Enaux et al., *Proc. Combust. Inst.* (2010), doi:10.1016/j.proci.2010.07.038

mixture composition (local equivalence ratio, dilution), thermodynamic conditions, turbulence or mean flow velocity in the spark plug vicinity among the most important ones. For the present computation, the local equivalence ratio is not a relevant parameter since the mixture is perfectly premixed. All other parameters vary notably from cycle to cycle and it is difficult to separate their respective influence. Some attempts to correlate the local dilution ratio or the temperature at spark timing with the combustion speed have revealed no clear tendency. On the contrary, the influence of the velocity field is much more evident. Figure 10 (left) shows velocity vectors in a cut plane through the spark plug at spark timing while Fig. 10 (right) shows the flame front 5 CAD later for the three cycles 14, 15 and 16. The comparison clearly highlights the importance of the residual tumble motion at spark timing since it determines in a large part how the initial kernel will develop with respect to the spark plug cavity. For cycles 14 and 15, the flow resulting from the tumble pushes the kernel towards the exhaust side. For cycle 16, the tumble motion is already on the exhaust side and the kernel is driven in the spark plug cavity. The consequences of this initial location of the flame kernel are multiple. Heat losses are more important (global heat losses integrated over the cylinder head walls during the first 10 CAD after ignition are 6% higher in cycle 16 compared to cycle 14) and partial quenching is more likely to occur if the kernel is completely confined. Moreover, the turbulence in the spark plug cavity is much less intense than in the rest of the combustion chamber. As an illustration, the evolution of the velocity fluctuations, u', integrated over the flame surface is displayed in Fig. 11. The definition of u' has been carefully chosen [22] in order not to account for the dilatational

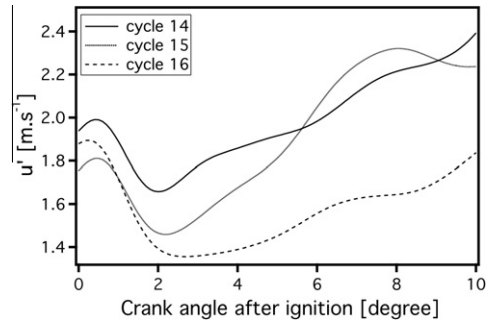

Fig. 11. Evolution of the velocity fluctuations integrated over the flame surface.

part of the velocity. Figure 11 shows that a cycle which experiences a slow combustion process (cycle 16) encounters level of u' much less intense in the first 10 CAD after ignition than fast cycles like cycles 14 and 15. Obviously, these mechanisms make the combustion speed lower if the kernel develops in the cavity and the resulting peak cylinder pressure will be also lower in this case.

As mentioned in Section 4.3, phase 3 also has a non negligible influence on the flame propagation. Contrary to phase 1, the main factor which triggers variations during this phase is unclear. Indeed, during this phase, the flame propagation depends not only on several physical parameters (turbulence level, temperature, flame/wall interaction...) but also on the history of the flame during the first two phases (location of the flame front at CA10 in particular), making the direct comparison cycle to cycle delicate. In any case, it is worth reminding that this phase can only deflect the initial trend for some cycles and not completely revert it. In the present configuration, the variability in the velocity field

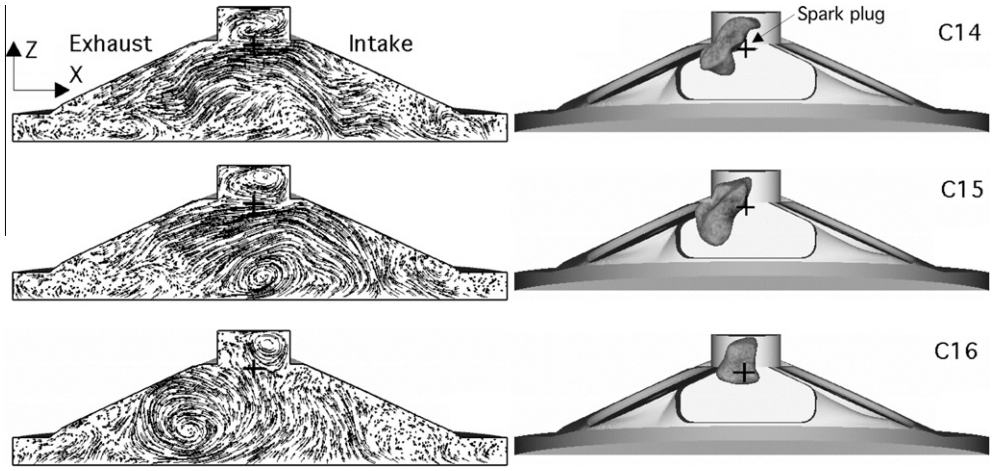

Fig. 10. Left: velocity vector at spark timing in a cut plane through the spark plug. Right: iso-surface of progress variable $c = 0.5$, 5 CAD after ignition.

Please cite this article in press as: B. Enaux et al., *Proc. Combust. Inst.* (2010), doi:10.1016/j.proci.2010.07.038

at spark timing seems thus clearly the main triggering factor for combustion variability.

5. Conclusion

The use of an experimental database tailored for LES validation has confirmed the high potential of LES to accurately capture cyclic combustion variations in piston engines. The stable nature of the considered operating point (relative variation in peak pressure <5%) and the range of variations have been correctly predicted. Investigations of the sources of CCV have shown that, in the present case, variations in the velocity field at the spark plug control the initial growth of the flame and determine to a large extent the overall combustion duration. These large-scale aerodynamic variations manifest themselves through changes in the location of the tumble residual motion at spark timing from cycle to cycle. For cycles with a non-centered tumble motion, the initial flame kernel is driven in the spark plug cavity where it undergoes higher heat losses and benefits from lower turbulence activity, resulting in slower flame development. This initial trend may be partly deflected afterwards, during the fully turbulent propagation phase but this phenomenon is more complex to interpret, due to the large number of parameters involved and due to the different history of the initial flame developments from cycle to cycle. Further investigations would also be required to determine the source of the observed tumble center precession and its possible link with the intake stroke or the CCV in the intake ports.

Acknowledgments

The authors gratefully acknowledge the financial support provided by PSA Peugeot Citroën and Renault SAS in the framework of thesis researches. This work was granted access to the HPC resources of CINES under the allocation 2009-c2009026055 made by GENCI (Grand Equipement National de Calcul Intensif). The authors acknowledge the financial support by ANR under grant N.ANR-06-PDIT-007-01 SGEmac.

References

[1] T. Lieuwen, V. Yang, Combustion instabilities in gas turbine engines: operational experience, fundamental mechanisms and modeling, *Prog. in Astronautics and Aeronautics AIAA*, vol. 210, 2005.
[2] Y. Huang, S. Wang, V. Yang, *AIAA J.* 44 (2006) 724–740.
[3] P. Schmitt, T. Poinsot, B. Schuermans, K. Geigle, *J. Fluid Mech.* 570 (2007) 17–46.
[4] A. Roux, L.Y.M. Gicquel, Y. Sommerer, T. Poinsot, *Combust. Flame* 152 (1-2) (2008) 154–176.
[5] O. Vermorel, S. Richard, O. Colin, C. Angelberger, A. Benkenida, D. Veynante, *Combust. Flame* 156 (2009) 1525–1541.
[6] D. Goryntsev, A. Sadiki, M. Klein, J. Janicka, *Proc. Combust. Inst.* 32 (2009) 2759–2766.
[7] S. Richard, O. Colin, O. Vermorel, C. Angelberger, A. Benkenida, D. Veynante, *Proc. Combust. Inst.* 31 (2) (2007) 3059–3066.
[8] C. Hasse, V. Sohm, B. Durst, *Comp. Fluids* 39 (1) (2010) 25–48.
[9] C. Lacour, C. Pera, B. Enaux, O. Vermorel, C. Angelberger, T. Poinsot, *Proc. of the Fourth European Combustion Meeting*, Vienna, 2009.
[10] V. Moureau, G. Lartigue, Y. Sommerer, C. Angelberger, O. Colin, T. Poinsot, *J. Comput. Phys.* 202 (2) (2005) 710–736.
[11] P. Lax, B. Wendroff, *Commun. Pure Appl. Math.* 13 (1960) 217–237.
[12] J. Smagorinsky, *Mon. Weather Rev.* 91 (1963) 99–164.
[13] V. Moureau, I. Barton, C. Angelberger, T. Poinsot, SAE Paper 2004-01-1995, 2004.
[14] V. Moureau, O. Vasilyev, C. Angelberger, T. Poinsot, *in: Proc. of the Summer Program, Center for Turbulence Research*, NASA AMES/Stanford Univ., 2004, pp. 157–168.
[15] T. Poinsot, S. Lele, *J. Comput. Phys.* 101 (1) (1992) 104–129.
[16] B. Enaux, V. Granet, O. Vermorel, et al., *Flow Turb. Combust.*, in press, doi:10.1007/s10494-010-9299-7.
[17] S. Mendez, J.D. Eldredge, *J. Comput. Phys.* 228 (13) (2009) 4757–4772.
[18] M. Metghalchi, J. Keck, *Combust. Flame* 38 (1980) 143–154.
[19] S. Jerzembeck, N. Peters, P. Pepiot-Desjardins, H. Pitsch, *Combust. Flame* 156 (2) (2009) 292–301.
[20] G.P. Smith, D.M. Golden, M. Frenklach, et al. Available from: <http://www.me.berkeley.edu/gri_mech/>.
[21] D.G. Goodwin, Cantera C++ Users Guide, 2002. Available from: <http://sourceforge.net/projects/cantera>.
[22] O. Colin, F. Ducros, D. Veynante, T. Poinsot, *Phys. Fluids* 12 (7) (2000) 1843–1863.
[23] G. Lacaze, B. Cuenot, T. Poinsot, M. Oschwald, *Combust. Flame* 156 (2009) 1166–1180.
[24] G. Lacaze, E. Richardson, T. Poinsot, *Combust. Flame* 156 (2009) 1993–2009.
[25] R. Maly, M. Vogel, *Proc. Combust. Inst.* 17 (1978) 821–831.
[26] R. Teets, J. Sell, *SAE Trans.* 97 (1988) 371–383.
[27] F. Nicoud, L. Benoit, C. Sensiau, T. Poinsot, *AIAA J.* 45 (2007) 426–441.
[28] N. Ozdor, M. Dulger, E. Sher, SAE Paper 950683, 1994.
[29] M.B. Young, SAE Paper 810020, 1981.